

Phase-coherent transport in InN nanowires of various sizes

Ch. Blömers,¹ Th. Schäpers,^{2,*} T. Richter,³ R. Calarco,¹ H. Lüth,¹ and M. Marso¹

¹*Institute for Bio- and Nanosystems (IBN-1) and JARA Jülich-Aachen Research Alliance, Research Centre Jülich GmbH, 52425 Jülich, Germany*

²*Institute for Bio- and Nanosystems (IBN-1), JARA Jülich-Aachen Research Alliance, and Virtual Institute of Spinelectronics (VISel), Research Centre Jülich GmbH, 52425 Jülich, Germany*

³*Institute for Bio- and Nanosystems (IBN-1) and JARA Jülich Aachen Research Alliance, Research Centre Jülich GmbH, 52425 Jülich, Germany*

(Dated: September 12, 2021)

We investigate phase-coherent transport in InN nanowires of various diameters and lengths. The nanowires were grown by means of plasma-assisted molecular beam epitaxy. Information on the phase-coherent transport is gained by analyzing the characteristic fluctuation pattern in the magneto-conductance. For a magnetic field oriented parallel to the wire axis we found that the correlation field mainly depends on the wire cross section, while the fluctuation amplitude is governed by the wire length. In contrast, if the magnetic field is oriented perpendicularly, for wires longer than approximately 200 nm the correlation field is limited by the phase coherence length. Further insight into the orientation dependence of the correlation field is gained by measuring the conductance fluctuations at various tilt angles of the magnetic field.

Semiconductor nanowires fabricated by a bottom-up approach^{1,2,3} have emerged as very interesting systems not only for the design of future nanoscale device structures^{4,5,6} but also to address fundamental questions connected to strongly confined systems. Regarding the latter, quantum dot structures,^{7,8,9} single electron pumps,¹⁰ or superconducting interference devices¹¹ have been realized. Many of the structures cited above were fabricated by employing III-V semiconductors, e.g. InAs or InP.¹ Apart from these more established materials, InN is particularly interesting for nanowire growth because of its low energy band gap and its high surface conductivity.^{12,13,14}

At low temperatures the transport properties of nanostructures are affected by electron interference effects, i.e. weak localization, the Aharonov–Bohm effect, or universal conductance fluctuations.^{15,16} The relevant length parameter in this transport regime is the phase coherence length l_ϕ , that is the length over which phase-coherent transport is maintained. In order to obtain information on l_ϕ , the analysis of conductance fluctuations is a very powerful method.^{17,18,19,20,21,22,23} In fact, in InAs nanowires pronounced fluctuations in the conductance have been observed and analyzed, recently.²⁴

Here, we report on a detailed study of the conductance fluctuations δG measured in InN nanowires of various sizes. Information on the phase-coherent transport is gained by analyzing the average fluctuation amplitude and the correlation field B_c . Special attention is drawn to the magnetic field orientation with respect to the wire axis, since this allowed us to change the relevant probe area for the detection of phase-coherent transport.

The InN nanowires investigated here were grown without catalyst on a Si (111) substrate by plasma-assisted MBE.^{14,25} The measured wires had a diameter d ranging from 42 nm to 130 nm. The typical wire length was 1 μm . From photoluminescence measurements an overall electron concentration of about $5 \times 10^{18} \text{ cm}^{-3}$ was

TABLE I: Dimensions and characteristic parameters of the different wires: Length L (separation between the contacts), wire diameter d , root-mean-square of the conductance fluctuations $\text{rms}(G)$, correlation field B_c . The latter two parameters were determined for B parallel to the wire axis.

Wire	L (nm)	d (nm)	$\text{rms}(G)$ (e^2/h)	B_c (T)
A	205	58	1.35	0.38
B	580	66	0.58	0.22
C	640	75	0.52	0.21
D	530	130	0.81	0.15

determined.²⁵

For the samples used in the transport measurements, first, contact pads and adjustment markers were defined on a SiO₂-covered Si (100) wafer. Subsequently, the InN nanowires were placed on the patterned substrate and contacted individually by Ti/Au electrodes. Four wires labeled as A, B, C, and D will be discussed in detail, below. Their parameters are summarized in Table I. In order to improve the statistics, additional wires which are not specifically labeled, were included in part of the following analysis. A micrograph of a typical contacted wire is depicted in Fig. 4 (inset).

The transport measurements were performed in a magnetic field range from 0 to 10 T at a temperature of 0.6 K. In order to vary the angle between the wire axis and the magnetic field B , the samples were mounted in a rotating sample holder. The rotation axis was oriented perpendicularly to the magnetic field and to the wire axis. The magnetoresistance was measured by using a lock-in technique with an ac bias current of 30 nA.

The fluctuation pattern for nanowires with different dimensions are depicted in Fig. 1(a). Here, the normalized conductance fluctuations δG for wires A to C comprising successively increasing diameters are plotted

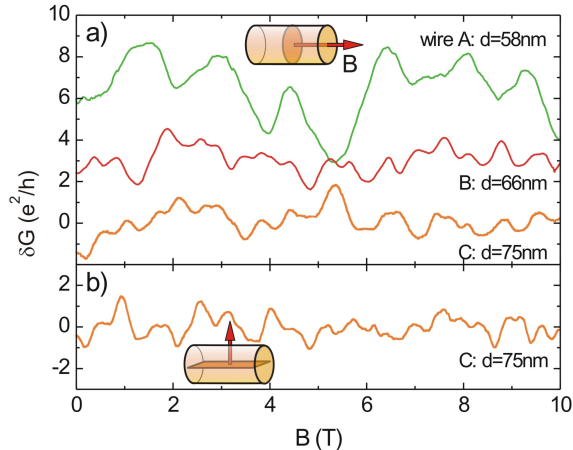


FIG. 1: (a) Conductance fluctuations normalized to e^2/h for wires with different length and diameter. The curves are offset for clarity. As illustrated by the sketch, the magnetic field is axially oriented. (b) Conductance fluctuations of wire C with a magnetic field oriented perpendicularly to the wire axis.

as a function of the magnetic field B . The field was oriented parallel to the wire axis. The measurements were performed up to a relatively large field of 10 T. This is justified, since even at 10 T the estimated cyclotron diameter of 70 nm just begins to become comparable to the wire diameter. The conductance variations were determined by first subtracting the typical contact resistance of $(330 \pm 50) \Omega$, and then converting the resistance variations to conductance variations. It can clearly be seen in Fig. 1(a), that for the narrowest and shortest wire, i.e. wire A, the conductance fluctuates with a considerably larger amplitude than for the other two wires with larger diameters and length. The parameter quantifying this feature is the root-mean-square of the fluctuation amplitude $\text{rms}(G)$ defined by $\sqrt{\langle \delta G^2 \rangle}$. Here, $\langle \dots \rangle$ represents the average over the magnetic field. For quasi one-dimensional systems where phase coherence is maintained over the complete wire length it is expected that $\text{rms}(G)$ is in the order of e^2/h .^{19,20,21} As one can infer from Table I, for the shortest nanowire, i.e. wire A, $\text{rms}(G)$ falls within this limit. For the other two wires the $\text{rms}(G)$ values are smaller than e^2/h (cf. Table I). Thus, for these wires it can be concluded that the phase coherence length l_ϕ , is smaller than the wire length L .

Beside $\text{rms}(G)$, another important parameter is the correlation field B_c , quantifying on which field scale the conductance fluctuations take place. The correlation field is extracted from the autocorrelation function of δG defined by $F(\Delta B) = \langle \delta G(B + \Delta B) \delta G(B) \rangle$.²¹ The magnetic field corresponding to half maximum of the autocorrelation function $F(B_c) = \frac{1}{2} F(0)$ defines B_c . The B_c values of the measurements shown in Fig. 1 are listed in Table I. Obviously, for wire A, which has the smallest diameter,

one finds the largest value of B_c . In a semiclassical approach it is expected that B_c is inversely proportional to the maximum area A_ϕ perpendicular to B which is enclosed phase-coherently:^{19,21,23}

$$B_c = \alpha \frac{\Phi_0}{A_\phi}. \quad (1)$$

Here, α is a constant in the order of one and $\Phi_0 = h/e$ the magnetic flux quantum. As long as phase coherence is maintained along the complete circumference, A_ϕ is equal to the wire cross section $\pi d^2/4$ and thus one expects $B_c \propto 1/d^2$. The B_c values given in Table I follow this trend, i.e. becoming smaller for increasing diameter d . As can be recognized in Fig. 2 (inset), $F(\Delta B)$ also shows negative values at larger ΔB . This behavior can be attributed to the limited number of modes in the wires, as it was observed previously for small size semiconductor structures.^{26,27} However, as discussed by Jalabert *et al.*²⁶, at small fields $F(\Delta B)$ and thus B_c being calculated fully quantum mechanically correspond well to the semiclassical approximation.

In order to elucidate the dependence of B_c on the wire diameter in more detail, a larger number of wires was measured. As can be seen in Fig. 2(a), B_c systematically decreases with d . Leaving out wire D which has the largest diameter, the decrease of B_c is well described by a $1/d^2$ -dependence. As mentioned above, for short wires ($L \approx 200$ nm) we found that phase coherence is maintained over the complete length. This length corresponds to a circumference of a wire with a diameter of about 64 nm. Except of wire D, d is in the order of that value, so that one can expect that phase coherence is maintained within the complete cross section. For the parameter α we found a value of 0.24, which is by a factor of 4 smaller than the theoretically expected value of 0.95.²³ Choosing $\alpha = 0.95$ would result in lower bound values of B_c being larger than all corresponding experimental values, which is physically unreasonable. We attribute the discrepancy to the different geometrical situation, i.e. for the latter a confined two-dimensional electron gas with a perpendicularly oriented magnetic field was considered,²³ while in our case the field is oriented parallel to the wire axis. In addition, an inhomogeneous carrier distribution within the cross section, e.g. due to a carrier accumulation at the surface,²⁸ can also result in a disagreement between experiment and theoretical model. As can be seen in Fig. 2(a) (inset), the data point of the wire with the largest diameter of 130 nm, i.e. wire D, is found above the calculated curve. This indicates that presumably for this sample, A_ϕ is slightly smaller than the wire cross section.

Next, we will focus on measurements of δG with a magnetic field oriented perpendicular to the wire axis. As a typical example, δG of wire C is shown in Fig. 1(b). Here, a correlation field of 0.17 T was extracted, which is smaller than the value of corresponding measurements with B parallel to the wire axis [c.f. Fig. 1(a) and Table I]. The smaller value of B_c can be attributed to the ef-

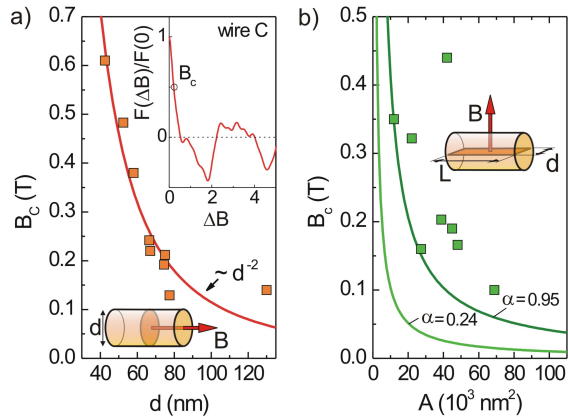


FIG. 2: (a) Correlation field B_c as a function of the wire diameter d . As illustrated in the schematics the magnetic field B was oriented axially. The solid lines corresponds to the calculated correlation field. The inset shows $F(\Delta B)/F(0)$ for wire C. (b) B_c as a function of the maximum area $A = Ld$ (see schematics) of the wire. The magnetic field is oriented perpendicular to the wire axis. The solid lines represents the calculated lower boundary correlation fields assuming $\alpha = 0.95$ and 0.24 , respectively.

fect that now the relevant area for magnetic flux-induced interference effects is no longer limited by the relatively small circular cross section but rather by a larger area within the rectangle defined by L and d , as illustrated by the schematics in Fig. 2(b).

In Fig. 2(b) the B_c values of various wires are plotted as a function of the maximum area $A_{max} = Ld$ penetrated by the magnetic field. As a reference, the calculated curve using Eq. (1) and assuming $A_\phi = A_{max}$ are also plotted. It can be seen that the B_c values of two wires with small areas, including wire A, match to the theoretically expected ones if one takes $\alpha = 0.95$, as given by Beenakker and van Houten.²³ This corresponds to the case of phase-coherent transport across the complete wire, as it was, in case of wire A, already concluded from the $\text{rms}(G)$ analysis. For all other wires the B_c values are above the theoretically expected curve, corresponding to the case $A_\phi < A_{max}$. At this point, one might argue that for B oriented along the wire axis a better agreement is found for $\alpha = 0.24$. However, as can be seen in Fig. 2(b), if one assumes $\alpha = 0.24$ all experimental values are above the calculated curve, i.e. $A_\phi < A_{max}$. This does not agree with the observation that for short wires $\text{rms}(G)$ is in the order of e^2/h . We attribute the difference between the appropriate α values for different field orientations to the different character of the relevant area penetrated by the magnetic flux, e.g. due to carrier accumulation at the surface.

Beside B_c we also analyzed the fluctuation amplitude for five different wires with B oriented perpendicular to

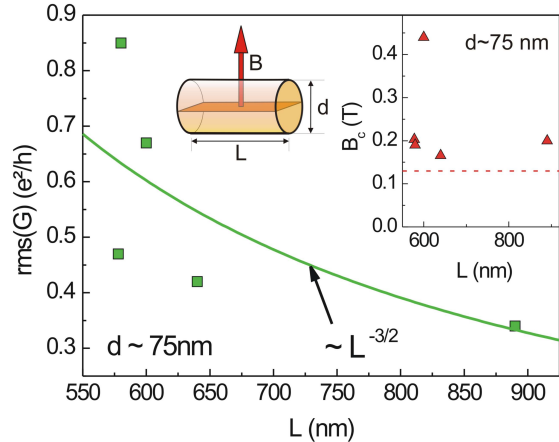


FIG. 3: $\text{rms}(G)$ for wires with a diameter of (75 ± 5) nm as a function of wire length L (square). The magnetic field is oriented perpendicular to the wire axis. The calculated decrease of $\text{rms}(G)$ proportional to $L^{-3/2}$ is plotted as solid line. The inset shows B_c vs. L for wires with $d \approx 75$ nm. The dashed line corresponds to the calculated value of B_c assuming $l_\phi = 430$ nm.

the wire axis. Only wires with comparable diameters of (75 ± 5) nm were chosen, here. It can be seen in Fig. 3 that $\text{rms}(G)$ tends to decrease with increasing wire length L . From the previous discussion of B_c it was concluded that for long wires, as it is the case here, $l_\phi < L$. In this regime $\text{rms}(G)$ is expected to depend on L as^{21,23}

$$\text{rms}(G) = \beta \frac{e^2}{h} \left(\frac{l_\phi}{L} \right)^{3/2}, \quad (2)$$

with β in the order of one. The above expression is valid as long as the thermal diffusion length $l_T = \sqrt{\hbar D/k_B T}$, is larger than l_ϕ . Here, D is the diffusion constant. From our transport data we estimated $l_T \approx 600$ nm at $T = 0.6$ K. As can be seen in Fig. 3, the available experimental data points roughly follow the trend of the calculated curve using Eq. (2) and assuming $l_\phi = 430$ nm and $\beta = 1$. For the limit $l_\phi < L$, a correlation field according to $B_c = 0.95\Phi_0/dl_\phi$ is expected.²¹ As confirmed in Fig. 2(b), most experimental values of B_c are close to the calculated one.

If one compares the $\text{rms}(G)$ values for wires with $d \approx 75$ nm and B oriented axially (not shown here) with the corresponding values for B oriented perpendicularly, one finds, that both are in the same range. Thus it can be concluded that the fluctuation amplitude does not significantly depend on the magnetic field orientation. This is in contrast to the correlation field, where one finds a systematic dependence on the orientation of B .

In order to discuss the latter aspect in more detail the correlation field was studied for various tilt angles θ of the magnetic field. Figure 4 shows B_c of sample D if θ is

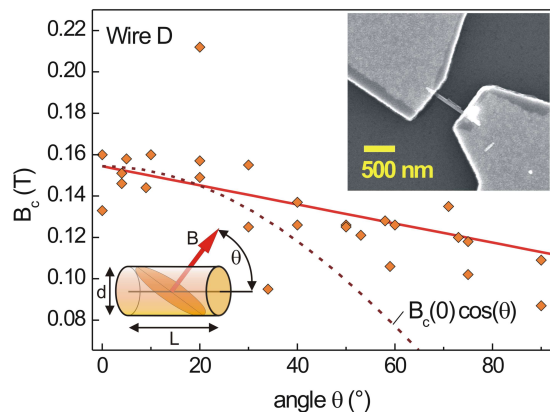


FIG. 4: Correlation field B_c of wire D as a function of the angle θ between the wire axis and B . The solid line represents a linear fit. The broken line corresponds to the theoretically expected B_c if phase-coherent transport is assumed in the complete wire. The left-hand-side inset shows a schematics of the geometrical situation. The right-hand-side inset shows a micrograph of a 580-nm-long wire with a diameter of 66 nm.

increased from 0° to 90° . The inset in Fig. 4 illustrates how θ is defined. Obviously, B_c decreases with increasing tilt angle θ . As explained above, the value of B_c is a measure of the maximum area normal to B , which is enclosed phase-coherently by the electron waves in the wire [see Fig. 4 (schematics)]. As long as $\theta \leq \arctan(L/d)$, this maximum area is given by $A(\theta) = \pi d^2/4 \cos \theta$. The expected θ -dependence of the correlation field is then given

by $B_c(\theta) = B_c(0) \cos(\theta)$, with $B_c(0)$ the correlation field at $\theta = 0$. As can be seen in Fig. 4, the calculated correlation field B_c , corresponding to fully phase-coherent transport, decreases much faster with increasing θ than the experimentally determined values. The experimental situation is better described by a linear decrease. As it was discussed above, at $\theta = 0$ one can assume that the area enclosed phase-coherently is equal to $A(0)$. However, if the tilt angle is increased the maximum wire cross section $A(\theta)$ presumably becomes larger than A_ϕ , resulting in a much smaller decrease of B_c than theoretically expected for fully phase-coherent transport. In addition, as pointed out above, the different tilt angles result in an angle-dependent parameter α . This is supported by the measurements of B_c for B parallel and perpendicular to the wire axis, where different values for α were determined, respectively.

In conclusion, the conductance fluctuations of InN nanowires with various lengths and diameters were investigated. We found that for an axially oriented magnetic field the correlation field B_c and thus the area where phase-coherent transport is maintained is limited by the wire cross section perpendicular to B . In contrast, $\text{rms}(G)$ decreases with the wire length, since this quantity also depends on the propagation of the electron waves along the wire axis. If the magnetic field is oriented perpendicularly we found that for long wires B_c is limited by l_ϕ rather than by the length L . Our investigations demonstrate that phase-coherent transport can be maintained in InN nanowires, which is an important prerequisite for the design of quantum device structures based on this material system.

* Electronic address: th.schaepers@fz-juelich.de

- ¹ C. Thelander, P. Agarwal, S. Brongersma, J. Eymery, L. Feiner, A. Forchel, M. Scheffler, W. Riess, B. Ohlsson, U. Gösele, et al., *Materials Today* **9**, 28 (2006).
- ² W. Lu and C. M. Lieber, *J. Phys. D: Appl. Phys.* **39**, R387 (2006).
- ³ K. Ikejiri, J. Noborisaka, S. Hara, J. Motohisa, and T. Fukui, *J. Cryst. Growth* **298**, 616 (2007).
- ⁴ M. T. Björk, B. J. Ohlsson, C. Thelander, A. I. Persson, K. Deppert, L. R. Wallenberg, and L. Samuelson, *Appl. Phys. Lett.* **81**, 4458 (2002).
- ⁵ T. Bryllert, L.-E. Wernersson, T. Lowgren, and L. Samuelson, *Nanotechnology* **17**, 227 (2006).
- ⁶ Y. Li, J. Xiang, F. Qian, S. Gradecak, Y. Wu, H. Yan, D. Blom, and C. M. Lieber, *Nano Letters* **6** (2006).
- ⁷ S. D. Franceschi, J. A. van Dam, E. P. A. M. Bakkers, L. Feiner, L. Gurevich, and L. P. Kouwenhoven, *Appl. Phys. Lett.* **83**, 344 (2003).
- ⁸ C. Fasth, A. Fuhrer, M. T. Bjork, and L. Samuelson, *Nanoletters* **5**, 1487 (2005).
- ⁹ A. Pfund, I. Shorubalko, R. Leturcq, and K. Ensslin, *Appl. Phys. Lett.* **89**, 252106 (2006).
- ¹⁰ A. Fuhrer, C. Fasth, and L. Samuelson, *Appl. Phys. Lett.* **91**, 052109 (2007).

- ¹¹ J. A. van Dam, Y. V. Nazarov, E. P. A. M. Bakkers, S. D. Franceschi, and L. P. Kouwenhoven, *Nature* **442**, 667 (2006).
- ¹² C. H. Liang, L. C. Chen, J. S. Hwang, K. H. Chen, Y. T. Hung, and Y. F. Chen, *Appl. Phys. Lett.* **81**, 22 (2002).
- ¹³ C.-Y. Chang, G.-C. Chi, W.-M. Wang, L.-C. Chen, K.-H. Chen, F. Ren, and S. J. Pearton, *Appl. Phys. Lett.* **87**, 093112 (2005).
- ¹⁴ R. Calarco and M. Marso, *Appl. Phys. A* **87**, 499 (2007).
- ¹⁵ C. W. J. Beenakker and H. van Houten, in *Solid State Physics*, edited by H. Ehrenreich and D. Turnbull (Academic, New York, 1991), vol. 44, p. 1.
- ¹⁶ J. J. Lin and J. P. Bird, *J. Phys.: Cond. Mat.* **14**, R501 (2002).
- ¹⁷ C. P. Umbach, S. Washburn, R. B. Laibowitz, and R. A. Webb, *Phys. Rev. B* **30**, 4048 (1984).
- ¹⁸ A. D. Stone, *Phys. Rev. Lett.* **54**, 2692 (1985).
- ¹⁹ P. A. Lee and A. D. Stone, *Phys. Rev. Lett.* **55**, 1622 (1985).
- ²⁰ B. Al'tshuler, *Pis'ma Zh. Eksp. Teo. Fiz. [JETP Lett.* **41**, 648-651 (1985)] **41**, 530 (1985).
- ²¹ P. A. Lee, A. D. Stone, and H. Fukuyama, *Phys. Rev. B* **35**, 1039 (1987).
- ²² T. J. Thornton, M. Pepper, H. Ahmed, G. J. Davies, and

- D. Andrews, Phys. Rev. B **36**, 4514 (1987).
- ²³ C. W. J. Beenakker and H. van Houten, Phys. Rev. B **37**, 6544 (1988).
- ²⁴ A. E. Hansen, M. T. Börk, C. Fasth, C. Thelander, and L. Samuelson, Phys. Rev. B **71**, 205328 (2005).
- ²⁵ T. Stoica, R. J. Meijers, R. Calarco, T. Richter, E. Sutter, and H. Lüth, Nano Lett. **6**, 1541 (2006).
- ²⁶ R. A. Jalabert, H. U. Baranger, and A. D. Stone, Phys. Rev. Lett. **65**, 2442 (1990).
- ²⁷ J. P. Bird, D. K. Ferry, R. Akis, Y. Ochiai, K. Ishsibashi, Y. Aoyagi, and T. Sugano, Europhys. Lett. **35**, 529 (1996).
- ²⁸ I. Mahboob, T. D. Veal, C. F. McConville, H. Lu, and W. J. Schaff, Phys. Rev. Lett. **92**, 036804 (2004).